Article:
Cowlam, N. and Wildes, A.R. (2011) Sperimagnetism in Fe(78)Er(5)B(17) and Fe(64)Er(19)B(17) metallic glasses: II. Collinear components and ferrimagnetic compensation. Journal of Physics: Condensed Matter, 23 (49). Art no. 496005. ISSN: 0953-8984

https://doi.org/10.1088/0953-8984/23/49/496005

Sperimagnetism in $Fe_{78}Er_5B_{17}$ and $Fe_{64}Er_{19}B_{17}$ metallic glasses. II – Collinear components and ferrimagnetic compensation.

N Cowlam[a] and A R Wildes[b]

[a]Department of Physics and Astronomy, University of Sheffield, SHEFFIELD, S3 7RH, U.K,

[b]Institut Laue-Langevin, BP 156, 6 rue jules Horowitz, 38042 GRENOBLE Cedex 9, France,

Abstract.

Magnetisation measurements on a $Fe_{64}Er_{19}B_{17}$ glass and polarised beam neutron scattering measurements on $Fe_{78}Er_5B_{17}$ and $Fe_{64}Er_{19}B_{17}$ were described in **Part I**. The finite spin-flip neutron scattering cross-sections were calculated using a sperimagnetic structure based on random cone arrangements of the magnetic moments. The temperature variation of the cross-sections of $Fe_{64}Er_{19}B_{17}$ suggested that a compensated sperimagnetic phase existed at T_{comp}.

The analysis of the non spin-flip neutron scattering cross-sections is described here in **Part II**. Two spin-dependent total structure factors $S^{\pm\pm}(Q)$ were defined from these cross-sections and despite the limited range of the data $0.5\text{Å}^{-1} < Q < 6.5\text{Å}^{-1}$, their Fourier transform gave reliable spin-dependent Radial Distribution Functions $RDF^{\pm\pm}(r)$. These were interpreted in terms of the atomic pair correlation functions $\rho_{AB}^{\pm\pm}(r)$ and their weighting factors $\omega_{AB}^{\pm\pm}$. The data on $Fe_{64}Er_{19}B_{17}$ at 1.5K showed for example, how the directions of the magnetic sublattices can be defined uniquely. The analysis of the $RDF^{\pm\pm}(r)$ for $Fe_{64}Er_{19}B_{17}$ at 112K confirmed that the mean collinear components of the magnetic moments $\langle \mu_{Er}^{\parallel} \rangle$, $\langle \mu_{Fe}^{\parallel} \rangle$ are zero on both sublattices in the compensated sperimagnetic structure at T_{comp}. The pre-peak in the spin-dependent total structure factors at 112K showed that it originated in the atomic structure and it may involve Fe-Er-Fe "collineations" at a radial distance of ≈ 6.0Å. Finally, the $RDF^{\pm\pm}(r)$ of $Fe_{64}Er_{19}B_{17}$ at 180K and of $Fe_{78}Er_5B_{17}$ at 2K, show that both glasses have the (μ_{Fe} **UP** : μ_{Er} **DOWN**) structure like the $(Fe,Tb)_{83}B_{17}$ collinear ferrimagnets.

1) Introduction

Our studies of the collinear and non-collinear magnetic structures in metallic glasses [1] were described in **Part I** [2], where it was explained that the non spin-flip neutron scattering cross-sections of $(Fe,Tb)_{83}B_{17}$ glasses had been simulated using a combination of known and derived partial structure factors [3]. The related $(Fe,Er)_{83}B_{17}$ glass have been shown to be a *non-collinear* ferrimagnets by a variety of different measurements [4, 5, 6, 7, 8], but our preliminary neutron scattering measurements on a $Fe_{64}Er_{19}B_{17}$ glass at 1.5K, 60K and 180K proved to be difficult to interpret [9]. The finite spin-flip cross-sections confirmed the presence of a non-collinear state and could be analysed using a sperimagnetic structure in which the magnetic moments on the iron atoms point in a random cone that is ferrimagnetically coupled to a random cone of erbium moments. However, the non spin-flip cross-sections were quite different from those of the parental $TM_{83}met_{17}$ glasses and strongly influenced by the 19% substitution of the large erbium ion with its large magnetic moment [9]. They could not be simulated by the method applied to the collinear $(Fe,Tb)_{83}B_{17}$ glasses [3].

The average components of the magnetic moments $\overline{\mu}^{\parallel}, \overline{\mu}^{\perp}$, parallel and perpendicular to the magnetic field are needed to describe the non spin-flip and spin-flip cross-sections respectively [1], so the variation of the magnetic moments must be known as a function of composition and temperature. In addition, there will be many different combinations of the values of the total moments $|\mu_{Fe}|$, $|\mu_{Er}|$ and the semi-vertex angles θ_{Fe}, θ_{Er} of their random cones in a non-collinear structure, which will lead to similar values of the $\overline{\mu}^{\parallel}$ and $\overline{\mu}^{\perp}$ components. It is difficult therefore, to find the *unique* choice of the components of the moments, even from a combination of different bulk measurements [4, 5, 6, 7, 8]. The aims of **Part I** of the present work were first to obtain magnetic moment values from magnetisation data on our own $Fe_{64}Er_{19}B_{17}$ glass, which we could use more confidently in the analysis of the neutron scattering. The neutron studies were also extended to include a second series of measurements on a $Fe_{78}Er_5B_{17}$ glass at 2K and on the $Fe_{64}Er_{19}B_{17}$ glass at 100K, 112K, 125K and again at 180K, as a consistency check. **Part II** will give an account of the ferrimagnetism in $Fe_{78}Er_5B_{17}$ glass at low temperature and of the magnetic structural changes that occur in $Fe_{64}Er_{19}B_{17}$ glass as a function of temperature. Sections 2 and 3 will cover the analysis of the non spin-flip cross-sections using a Fourier transform. This provides a

successful description of the atomic-scale structures in the two glasses, which works even when the magnetic contributions to the neutron scattering are small, such as when concentration of erbium is small (in $Fe_{78}Er_5B_{17}$ at 2K) or at higher temperatures (in $Fe_{64}Er_{19}B_{17}$ at 180K). The analysis of the scattering cross-sections by a Fourier transform involves no adjustable parameters, since the cross-sections were measured *in absolute units* and it relies solely on the values of the magnetic moments obtained in **Part I.**

2.0) The non spin-flip cross-sections of the $(Fe,Er)_{83}B_{17}$ glasses.

The two *non spin-flip cross-sections* are given in the usual notation in Equation 1 where b_i is the average coherent scattering length of atom i and $\frac{\partial\sigma_{II}}{\partial\Omega}$ is the isotope incoherent cross-section. Equation 1 may be compared with the spin-flip cross-sections given in Equation 6 in **Part I**.

$$\frac{\partial\sigma^{\pm\pm}}{\partial\Omega} = \frac{\partial\sigma_{II}}{\partial\Omega} + \frac{1}{3}\frac{\partial\sigma_{NSI}}{\partial\Omega} + \left|\left\langle \sum_{ij}\left(b_i \mp p_i^{\parallel}(Q)\right)\left(b_j^{*} \mp p_j^{\parallel^{*}}(Q)\right)\exp\left(iQ.\left(r_i - r_j\right)\right)\right\rangle\right|. \qquad (1)$$

The non spin-flip cross-sections contain the *collinear components* $p^{\parallel}(Q)$ of the magnetic scattering amplitude. They have a variation with scattering vector Q which is similar to the total structure factor $S(Q)$ of the glass, since they depend on the Fourier transform of spatial variation of either the sum $\frac{\partial\sigma^{--}}{\partial\Omega} \propto \left\langle FT\left(b + p^{\parallel}(Q)\right)\right\rangle^2$ or the difference $\frac{\partial\sigma^{++}}{\partial\Omega} \propto \left\langle FT\left(b - p^{\parallel}(Q)\right)\right\rangle^2$ of the nuclear and magnetic scattering amplitudes.

Figure 1 shows the non spin-flip cross-sections in absolute units of barns steradian^{-1} atom^{-1} for the $Fe_{78}Er_5B_{17}$ glass measured at 2K and for $Fe_{64}Er_{19}B_{17}$ measured at 1.5K, 60K, [9] and 100K, 112K, 125K, 180K. Only the present measurement at 180K has been plotted, as in **Part I**. The red and the blue points define the $\frac{\partial\sigma^{--}}{\partial\Omega}$ and $\frac{\partial\sigma^{++}}{\partial\Omega}$ cross-sections respectively. Two spin-dependent total structure factors $S^{--}(Q)$ and $S^{++}(Q)$ will be defined from these cross-sections in Section 2.1, so the peak in the cross-sections at $Q \approx 3$Å^{-1} will be called the first or main peak and the one (in just one channel) at $Q \approx 1.3$Å^{-1} will be the "pre-peak". This

follows the usual practice for the structure factors of metallic glasses. The large differences between the $\frac{\partial\sigma^{--}}{\partial\Omega}$ and $\frac{\partial\sigma^{++}}{\partial\Omega}$ cross-sections in Figure 1 arise because the combined

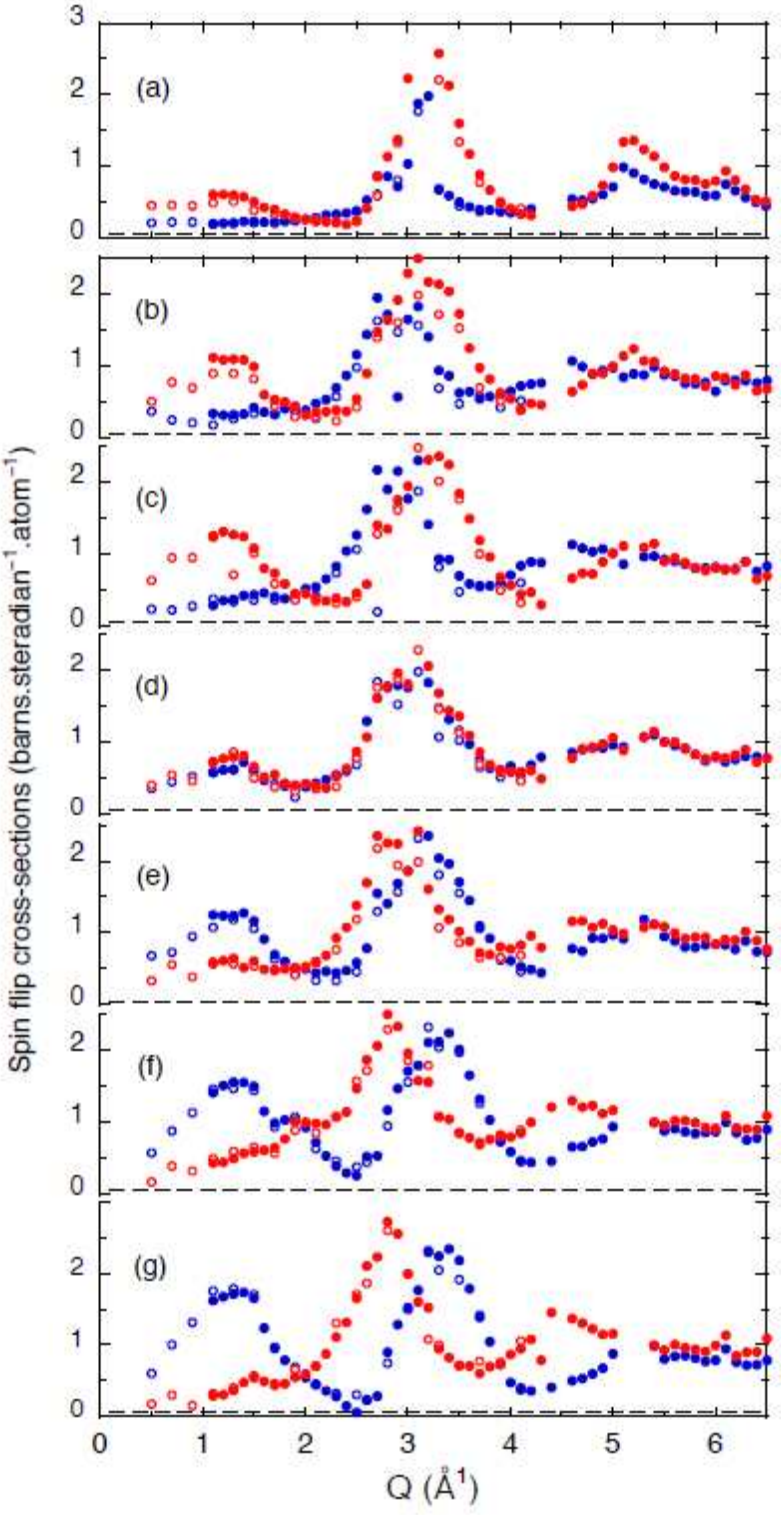

Figure 1 The non spin-flip cross-sections for the $Fe_{78}Er_5B_{17}$ glass at 2K are shown in 1a and for the $Fe_{64}Er_{19}B_{17}$ glass at 180K in 1b, 125K 1c, 112K 1d, 100K 1e, 60K 1f[9] and 1.5K

1g[9]. The red and blue points define the $\frac{\partial\sigma^{--}}{\partial\Omega}$ and $\frac{\partial\sigma^{++}}{\partial\Omega}$ cross-sections and the open and closed points are for incident wave vectors k_i = 2.662Å^{-1}, k_i = 4.1Å^{-1}. The incoherent cross-section is shown by a dashed line.

scattering amplitudes have a very large range of both positive and negative values, depending on how the scattering from the nucleus and from the magnetic electrons combine [10]. The nuclear scattering amplitudes are

$$b_{Fe} = 9.45\text{fm},\ b_{Er} = 7.79\text{fm and } b_B = 5.30 - 0.213i\ \text{fm [11]}$$

and substituting the moment values at 1.5K $\left|\overline{\mu}_{Fe}^{\parallel}\right| = 1.52\mu_B$ and $\left|\overline{\mu}_{Er}^{\parallel}\right| = 6.58\mu_B$ into $p^{\parallel}(Q) = 2.695\mu^{\parallel} f(Q)$ fm, gives the magnetic scattering amplitudes of $\left|p_{Fe}^{\parallel}(0)\right| = 4.10$ fm and $\left|p_{Er}^{\parallel}(0)\right| = 17.73$ fm in the forward limit Q=0, so that,

$$5.35\text{fm} < \left(b_{Fe} \mp p_{Fe}^{\parallel}(0)\right) < 13.55\text{fm} \quad \text{and} \quad -9.94\text{fm} < \left(b_{Er} \mp p_{Er}^{\parallel}(0)\right) < 25.52\text{fm}.$$

In Figure 1, the difference in position of the first peak in the $\frac{\partial\sigma^{--}}{\partial\Omega}$ and $\frac{\partial\sigma^{++}}{\partial\Omega}$ cross-sections of $Fe_{64}Er_{19}B_{17}$ at 1.5K, 60K and 100K is large ≈ 0.5Å^{-1} and the pre-peak occurs in $\frac{\partial\sigma^{++}}{\partial\Omega}$. The shapes of these cross-sections and the positions and widths of their peaks remain fairly constant and there is a reduction in the first peak in $\frac{\partial\sigma^{--}}{\partial\Omega}$ and the pre-peak with increasing temperature. In contrast, the $\frac{\partial\sigma^{--}}{\partial\Omega}$ and $\frac{\partial\sigma^{++}}{\partial\Omega}$ cross-sections have interchanged at 125K and 180K, when compared with those at low temperatures and this is shown clearly in the figure. The two first peaks in $\frac{\partial\sigma^{--}}{\partial\Omega}$ and $\frac{\partial\sigma^{++}}{\partial\Omega}$ have also moved closer together; their magnitudes have reduced and the first peak in $\frac{\partial\sigma^{++}}{\partial\Omega}$ is the smallest. The pre-peak (in $\frac{\partial\sigma^{--}}{\partial\Omega}$) is also smaller than the corresponding peak at $T \leq$ 100K. The interchange of cross-sections shows that there is a complete inversion of the magnetic structure between 100K and 125K. Comparison with the cross-sections of the $(Fe,Tb)_{83}B_{17}$ collinear ferrimagnets [3] suggests that at high temperatures the iron sublattice points along the field direction and the erbium sublattice is antiparallel to it (μ_{Fe} **UP** : μ_{Er} **DOWN**) and the inverted case (μ_{Fe} **DOWN** : μ_{Er} **UP**). occurs at low temperatures.

The constancy of shape of these cross-sections with temperature was monitored by superimposing the $\frac{\partial\sigma^{++}}{\partial\Omega}$ at 125K on to the $\frac{\partial\sigma^{--}}{\partial\Omega}$ at 100K and the $\frac{\partial\sigma^{++}}{\partial\Omega}$ at 100K on to the $\frac{\partial\sigma^{--}}{\partial\Omega}$ at 125K. The mean fractional differences in the data points in the superimposed cross-sections was less than ≈ 10%, - which is commensurate with the differences in the total scattering levels and in the ω_{AB}^{++} and ω_{AB}^{--} weighting factors (see below) at the two temperatures.

The $\frac{\partial\sigma^{++}}{\partial\Omega}$ and $\frac{\partial\sigma^{--}}{\partial\Omega}$ cross-sections measured at 112K are quite different from the others because they are virtually identical within the error bars, (except perhaps for four points near the pre-peak). Their first peak reaches ≈ 1.8 barns steradian^{-1} atom^{-1} and is slightly smaller than the first peak in the cross-sections measured at 100K and 125K. The pre-peak at $Q_{pp} \approx 1.3\text{Å}^{-1}$ occurs in both $\frac{\partial\sigma^{++}}{\partial\Omega}$, $\frac{\partial\sigma^{--}}{\partial\Omega}$ cross-sections with a height ≈ 0.75 barns steradian^{-1} atom^{-1} and the second peak has no shoulder. Equation 1 and Figure 5 of **Part I** show that the $\frac{\partial\sigma^{++}}{\partial\Omega}$ and $\frac{\partial\sigma^{--}}{\partial\Omega}$ cross-sections will be identical when the mean collinear components of the magnetic scattering amplitude tend to zero,

$$p^{\parallel}(Q) \to 0, \quad \text{so that} \quad \left\langle \left(b \mp p^{\parallel}(Q)\right)^2 \right\rangle \to \left\langle b^2 \right\rangle .$$

They will then contain information about the *atomic* structure of the glass, because they depend on the nuclear neutron scattering alone.

The $\frac{\partial\sigma^{++}}{\partial\Omega}$ and $\frac{\partial\sigma^{--}}{\partial\Omega}$ cross-sections for the $Fe_{78}Er_5B_{17}$ glass measured at 2K are shown in Figure 1a. They are similar to some of the first spin-dependent cross-sections which were measured for metallic glasses, such as $Co_{81}P_{19}$ [12], $Co_{81.5}B_{18.5}$ [13] and $Fe_{83}B_{17}$ [14] and also to the non spin-flip cross-sections of some of the $(Fe,Tb)_{83}B_{17}$ glasses [3]. The first peak in $\frac{\partial\sigma^{--}}{\partial\Omega}$ is much larger than that in $\frac{\partial\sigma^{++}}{\partial\Omega}$ and there is a clear difference in their positions. The $\frac{\partial\sigma^{--}}{\partial\Omega}$ cross-section also includes a very small pre-peak. The form of these $\frac{\partial\sigma^{--}}{\partial\Omega}$ and

$\frac{\partial\sigma^{++}}{\partial\Omega}$ cross-sections suggests that the $Fe_{78}Er_5B_{17}$ glass has the (μ_{Fe} **UP** : μ_{Er} **DOWN**) magnetic structure at 2K.

2.1) Spin-dependent total structure factors.

Two spin-dependent total structure factors $S^{--}(Q)$ and $S^{++}(Q)$ can be defined from the non spin-flip cross-sections and their Fourier Transform will in principle, provide information on the real space structures of the $(Fe,Er)_{83}B_{17}$ glasses. Initially, we did not believe it was realistic to try this because of the limited range $0.5\text{Å}^{-1} < Q < 6.5\text{Å}^{-1}$ of the IN20 data. It is smaller than the range $1\text{Å}^{-1} < Q < 12\text{Å}^{-1}$ used in the first polarised neutron scattering determination of the PSFs of the $Co_{81}P_{19}$ alloy [12] and its maximum value is much smaller than the $Q_{max} \approx 25\text{Å}^{-1}$ used in current studies of the structures of metallic glasses. An alternative is to make a simulation of the non spin-flip cross-sections by using known partial structure factors (PSF) and derived PSFs when the required ones are unavailable. This worked well for $(Fe,Tb)_{83}B_{17}$ glasses and correctly predicted the difference in the positions of the first peak in four pairs of non spin-flip cross-sections [3]. There are however, no PSFs which can generate the pre-peak in the non spin-flip cross-sections of the $Fe_{64}Er_{19}B_{17}$ glass, even after scaling their Q axis [9]. It seemed worthwhile therefore, to try a Fourier transform beginning with the non spin-flip cross-sections of the $Fe_{64}Er_{19}B_{17}$ glass at 1.5K which have the largest contribution from the magnetic scattering.

The derivation of the spin-dependent total structure factors is illustrated in Figure 2. The calculated total scattering levels (per atom) $\left\langle \left(b \mp p^{\parallel}(Q)\right)^2 \right\rangle$ are superimposed on the measured cross-sections in Figure 2a. The Q-dependence of the these levels is from the magnetic form factors within the $p^{\parallel}(Q)$ terms, described using the same seven parameter fits to the form factors of the Fe^{3+} and Er^{3+} ions [15] as in **Part I**. Note that the two levels have similar values in the forward limit $\left\langle \left(b + p^{\parallel}(0)\right)^2 \right\rangle$ = 1.46 barns steradian^{-1} atom^{-1} : $\left\langle \left(b - p^{\parallel}(0)\right)^2 \right\rangle$ = 1.41 barns steradian^{-1} atom^{-1} and both decrease towards, $\left\langle b^2 \right\rangle$ = 0.722 barns steradian^{-1} atom^{-1} at high Q. The measured cross-sections are greater than the total scattering level at some values of Q and less than it at others as expected. This Figure illustrates the crucial first step in the derivation of the spin-dependent structure factors, because the superposition of the calculated lines on the data points confirms that the cross-sections have been derived correctly in

absolute units. There are no adjustable parameters in these calculations, because the values of the b's are tabulated [11] and the $p^{\parallel}_{Fe}(Q)$, $p^{\parallel}_{Er}(Q)$ components have already been fixed in Table 1 of **Part I**.

The two spin-dependent structure factors can be defined by

$$S^{\pm\pm}(Q) = \frac{\frac{\partial\sigma^{\pm\pm}}{\partial\Omega} - \frac{\partial\sigma_{II}}{\partial\Omega} - \frac{1}{3}\frac{\partial\sigma_{NSI}}{\partial\Omega}}{\left\langle \left(b \mp p^{\parallel}(Q)\right)^2 \right\rangle}, \qquad (2)$$

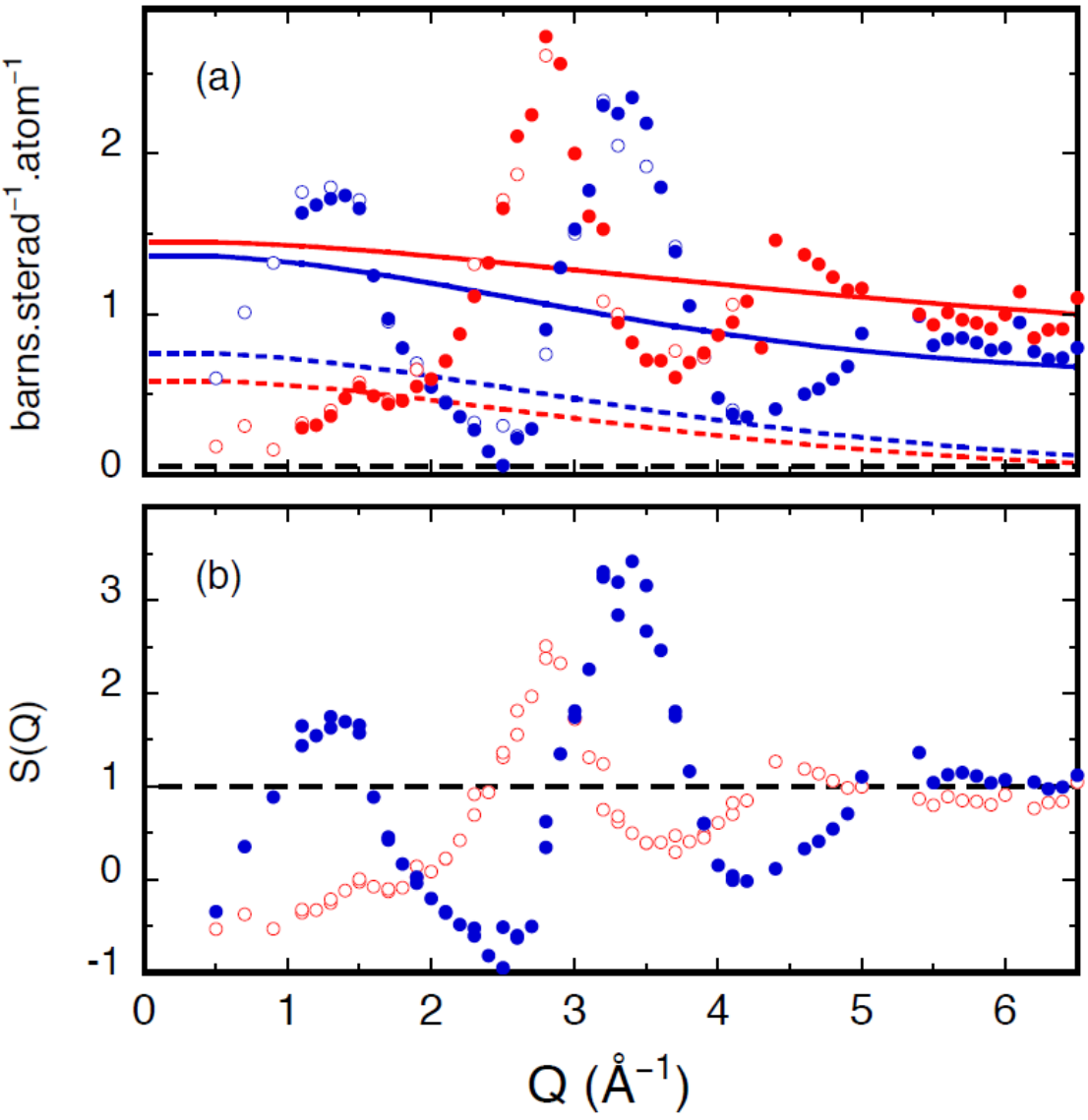

Figure 2 The non spin-flip cross-sections of the $Fe_{64}Er_{19}B_{17}$ glass at 1.5K are replotted in Figure 2a. The two continuous lines mark the total scattering levels; the two dashed lines the Laue-type scattering and the horizontal dashed line is the incoherent cross-section. The two

spin-dependent total structure factors $S^{--}(Q)$ and $S^{++}(Q)$ derived from these cross-sections are shown in Figure 2b.

but it is more convenient to normalise them on the coherent, rather than the total scattering,

$$S^{\pm\pm}(Q) = \frac{\frac{\partial\sigma^{\pm\pm}}{\partial\Omega} - \frac{\partial\sigma_{II}}{\partial\Omega} - \frac{1}{3}\frac{\partial\sigma_{NSI}}{\partial\Omega} \quad - \quad \left[\left\langle \left(b \mp p^{\parallel}(Q)\right)^2 \right\rangle - \left\langle \left(b \mp p^{\parallel}(Q)\right) \right\rangle^2\right]}{\left\langle \left(b \mp p^{\parallel}(Q)\right) \right\rangle^2}. \qquad (3)$$

The term in square brackets is the (Laue-type) disorder scattering which arises from the presence of two (or more) different atoms in the sample, - which here also have different values of magnetic moment. Subtracting the Laue-type scattering level, which is also shown in Figure 2a, and using Equation 3, allows the Faber-Ziman PSFs $S_{AB}(Q)$ [16] to be used to describe the atomic (AB) pair correlations in the glass,

$$\left\langle \left(b \mp p^{\parallel}(Q)\right) \right\rangle^2 S^{\pm\pm}(Q) = \sum_{AB} c_A c_B \left(b_A \mp p_A^{\parallel}(Q)\right)\left(b_B \mp p_B^{\parallel}(Q)\right) S_{AB}(Q). \qquad (4)$$

Here $c_A\, c_B$ are the concentrations, so that,

$$S^{\pm\pm}(Q) = \omega_{FeFe}^{\pm\pm} S_{FeFe}(Q) + \omega_{FeB}^{\pm\pm} S_{FeB}(Q) + \omega_{BB}^{\pm\pm} S_{BB}(Q) +$$

$$\omega_{FeEr}^{\pm\pm} S_{FeEr}(Q) + \omega_{ErB}^{\pm\pm} S_{ErB}(Q) + \omega_{ErEr}^{\pm\pm} S_{ErEr}(Q). \qquad (5)$$

The $\omega_{AB}^{\pm\pm}$ weighting factors are of the form,

$$\omega_{AA}^{\pm\pm} = \frac{c_A^2 \left(b_A \mp p_A^{\parallel}(Q)\right)^2}{\left\langle b \mp p^{\parallel}(Q) \right\rangle^2} \quad \text{and,}$$

$$\omega_{AB}^{\pm\pm} = \frac{2\, c_A c_B \left(b_A \mp p_A^{\parallel}(Q)\right)\left(b_B \mp p_B^{\parallel}(Q)\right)}{\left\langle b \mp p^{\parallel}(Q) \right\rangle^2}. \qquad (6)$$

Figure 2b shows the two spin-dependent total structure factors $S^{--}(Q)$ and $S^{++}(Q)$ obtained by calculating the total and Laue-type scattering at the same Q values as the data points in the non spin-flip cross-sections. They are shown with the same coding as the cross-sections. The $S^{--}(Q)$ structure factor is of conventional form, with a broad first peak at Q_1 = 2.8Å^{-1} and (possibly) a second peak at Q_2 ≈ 4.6Å^{-1}. It is similar to the $S_{FeFe}(Q)$ shown in Figure 3 of [9]. The $S^{++}(Q)$ structure factor has its pre-peak at Q_{pp} = 1.3Å^{-1}; a first peak at Q_1 = 3.3Å^{-1} and possibly a second peak at Q_2 ≈ 5.3Å^{-1}. It resembles the $S_{NiNi}(Q)$ shown in Figure 3 of [9] - except that the *relative* positions of the first peak and pre-peak are quite

different, $Q_1/Q_{pp} \approx 1.60$ for $S_{NiNi}(Q)$ and $Q_1/Q_{pp} \approx 2.54$ for $S^{++}(Q)$. This difference confirms that it is not possible to simulate the non spin-flip cross-sections of the $(Fe,Er)_{83}B_{17}$ glasses even when using those PSFs from the earlyTM-lateTM glasses which contain pre-peaks.

2.2) Spin-dependent Radial Distribution Functions

The Fourier transform of the $S^{\pm\pm}(Q)$ total structure factors gives (spin-dependent) reduced radial distribution functions $G^{\pm\pm}(r)$

$$G^{\pm\pm}(r) = \frac{2}{\pi} \int_0^{Q_{\max}} Q\left(S^{\pm\pm}(Q) - 1\right) \sin Qr\, M(Q)\, dQ\,, \tag{7}$$

where $M(Q)$ is a modification function, often of the form $\exp(-B\,Q^2)$, which reduces the effect of the finite value of Q_{max} in the Fourier transform. The corresponding Radial Distribution Functions $RDF^{\pm\pm}(r)$ are,

$$RDF^{\pm\pm}(r) = 4\pi r^2 \rho^{\pm\pm}(r) = r\,G^{\pm\pm}(r) + 4\pi r^2 \rho_0\,, \tag{8}$$

where ρ_0 is the mean atomic number density. The Fourier transform was made with an in-house program with summations over the 75 data points for $0 < Q < 6.5\text{Å}^{-1}$ and 80 points in r with intervals of $\Delta r = 0.1$Å for $0 < r < 4$Å and $\Delta r = 0.3$Å for $0 < r < 16$Å, using $M(Q) = \exp(-0.05Q^2)$. When a structure factor $S(Q)$ has been defined 100% correctly, the resulting $G(r)$ will be linear at small values of r where $\rho^{\pm\pm}(r) = 0$ and follow $-4\pi\rho_0 r$. This was found to be the case for the $Fe_{64}Er_{19}B_{17}$ glass at 1.5K and 180K, with slightly less good behaviour for $Fe_{64}Er_{19}B_{17}$ at 112K and $Fe_{83}Er_5B_{17}$ at 2K. The so-called "termination ripples" which appear in the $G^{\pm\pm}(r)$ at small r can be reduced by refining the levels $S(Q) = 0$ and $S(Q) = 1$ [17], but since no adjustable parameters had been introduced so far, this was not attempted. In fact, all the Fourier Transforms give a sufficiently clear picture of the structures of these glasses without the need for modification, as will be shown below.

3.0) Sperimagnetism in $Fe_{64}Er_{19}B_{17}$ glass at 1.5K.

Figure 3 shows the two functions $RDF^{++}(r)$ and $RDF^{--}(r)$ and are plotted over $0 < r <$ 6Å to illustrate the first neighbour peak, whose positions are $r_1^{++} = 2.43$Å in $RDF^{++}(r)$ and

r_1^{--} = 3.11Å in $RDF^{--}(r)$. This difference is consistent with the positions of the first peaks in their respective structure factors.

There is a large difference in the depth of the minimum after the first peak in the two *RDF*s, which is a real effect, since the two structure factors have the same value of Q_{max} and their *RDF*s have the same resolution in real space. The minimum in $RDF^{++}(r)$ actually goes slightly negative for just two points near $r \approx 3.3$Å and this will be discussed below. The first minimum in $RDF^{--}(r)$ is so shallow that the half-width of the first peak cannot be measured easily, - although it is about twice the width of the first peak in $RDF^{++}(r)$, $\Delta r_1^{++} \approx 0.9$Å. This also makes the coordination number n_1^{--} more difficult to obtain, except by measuring the area to the maximum of the first peak and doubling it, or by gradually removing the modification function *M(Q)* from the Fourier transform to improve the resolution. These two methods converge towards the values $n_1^{--} \approx 12.0$ and $n_1^{++} \approx 10.5$ and the first of these is consistent with dense packing in a metallic glass.

The expected first neighbour correlations in the $(Fe,Er)_{83}B_{17}$ glasses can be depicted by superimposing the familiar "stick diagrams" on to the first peak in the *RDF*s. Six atomic pair correlation functions $\rho_{AB}^{\pm\pm}(r)$ contribute to the *RDF* of the ternary $(Fe,Er)_{83}B_{17}$ glasses through a relation similar to Equation 5,

$$RDF^{\pm\pm}(r) = 4\pi r^2 [\omega_{FeFe}^{\pm\pm}\rho_{FeFe}(r) + \omega_{FeB}^{\pm\pm}\rho_{FeB}(r) + \omega_{BB}^{\pm\pm}\rho_{BB}(r) + \omega_{FeEr}^{\pm\pm}\rho_{FeEr}(r) + \omega_{ErB}^{\pm\pm}\rho_{ErB}(r) + \omega_{ErEr}^{\pm\pm}\rho_{ErEr}(r)]. \quad (9)$$

The $\omega_{AB}^{\pm\pm}$ weighting factors are as defined in Equation 6. The radial *positions* r_{AB} for these

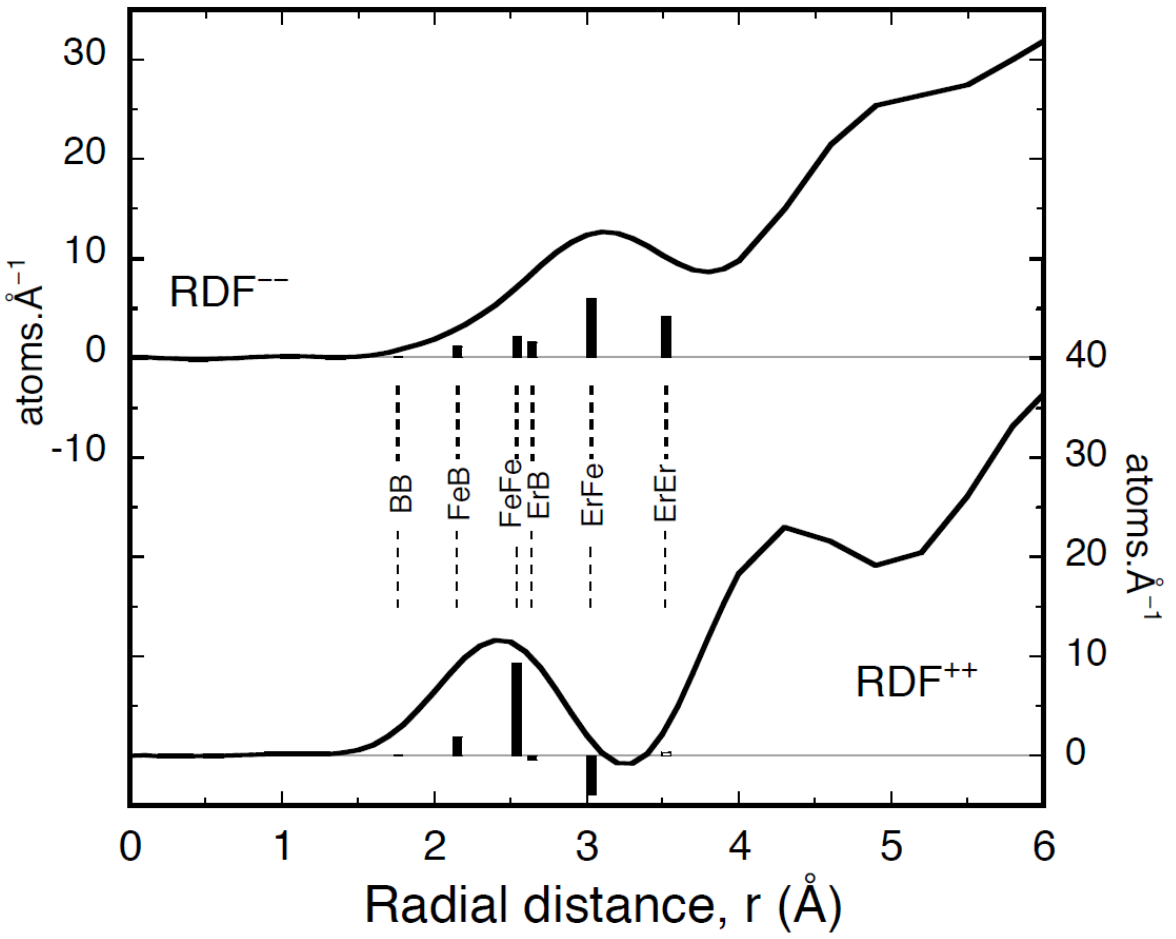

Figure 3 The spin-dependent radial distribution functions $RDF^{--}(r)$, $RDF^{++}(r)$ of the $Fe_{64}Er_{19}B_{17}$ glass at 1.5K are plotted over the range $0 < r < 6$Å to illustrate the first neighbour peak. The stick diagrams were drawn with the $\omega_{AB}^{\pm\pm}$ weighting factors from Table 1 corresponding to the (μ_{Fe} **DOWN** : μ_{Er} **UP**) structure.

"sticks" were obtained from the Goldschmidt radii of iron and erbium and the tetrahedral covalent radius of boron and are given in Table 1. The probability of finding an atom at a given point is proportional to its concentration when the structure of a glass is random. The $\omega_{AB}^{\pm\pm}$ weighting factors contain the concentrations of the species and their scattering amplitudes, so with a suitable multiplying factor, they can define the *height* of each stick in the case of a disordered structure. The values of the $\omega_{AB}^{\pm\pm}$ are given in Table 1 for two different configurations of the magnetic structure, with the iron sublattice pointing along the magnetic field direction, (μ_{Fe} **UP** : μ_{Er} **DOWN**) and the inverted case (μ_{Fe} **DOWN** : μ_{Er} **UP**). The magnetic scattering amplitude of erbium $p_{Er}^{\parallel}(Q)$ is so large that $\left(b_{Er} - p_{Er}^{\parallel}(Q)\right)$ and the ω_{ErB} and ω_{ErFe} weighting factors are negative, as discussed in Section 2.0. These positive and negative values of the $\omega_{AB}^{\pm\pm}$ weighting factors are the key feature in interpreting the position

and the shape of the first peak in the $RDF^{++}(r)$ and $RDF^{--}(r)$. Table 1 shows that when the magnetic structure inverts and the $p^{\parallel}_{Fe}(Q)$, $p^{\parallel}_{Er}(Q)$ both change sign, then the six ω^{++}_{AB} and ω^{--}_{AB} factors just exchange their values.

		$\omega^{\pm\pm}_{AB}$ weighting factors for $Fe_{64}Er_{19}B_{17}$ at 1.5K				
		Magnetic structure μ_{Fe} **DOWN** μ_{Er} **UP**			Magnetic structure μ_{Fe} **UP** & μ_{Er} **DOWN**	
Pair correlation	r_{AB} in Å	for $RDF^{--}(r)$ (*b*+*p*) type	for $RDF^{++}(r)$ (*b*-*p*) type		for $RDF^{--}(r)$ (*b*+*p*) type	for $RDF^{++}(r)$ (*b*-*p*) type
B-B	1.76	0.010	0.014		0.014	0.010
Fe-B	2.15	0.074	0.260		0.260	0.074
Fe-Fe	2.54	0.142	1.245		1.245	0.142
Er-B	2.64	0.103	-0.054		-0.054	0.103
Fe-Er	3.03	0.396	-0.519		-0.519	0.396
Er-Er	3.52	0.275	0.054		0.054	0.275

Table 1 The interatomic pair distances r_{AB} are given in ascending order with the ω_{AB} weighting factors calculated for the $Fe_{64}Er_{19}B_{17}$ at 1.5K, which are required to draw the "stick diagrams" on the first neighbour peak in the $RDF^{--}(r)$ and $RDF^{++}(r)$ radial distribution functions. The two columns of the ω^{++}_{AB} and ω^{--}_{AB} weighting factors interchange when the magnetic structure is inverted and $p^{\parallel}_{Fe}(Q)$, $p^{\parallel}_{Er}(Q)$ both change sign.

The stick diagrams calculated with the "correct" magnetic structure at 1.5K, (μ_{Fe} **DOWN** : μ_{Er} **UP**) superimposed on the appropriate $RDF^{--}(r)$, $RDF^{++}(r)$ curves in Figure 3. The first peak of the $RDF^{--}(r)$ provides a good envelope of the six first neighbour sticks and since they are all positive the coordination number ($n_1^{--} \approx 12.0$) derived from this peak should be correct. The dominant Fe-Er correlations at r_{FeEr} = 3.03Å determine the first neighbour distance r_1^{--} = 3.11Å, while the strong Er-Er correlations at r_{ErEr} = 3.52Å lift the $RDF^{--}(r)$ curve in the region of its first minimum as observed. The dominant correlations in the $RDF^{++}(r)$ curve are r_{FeFe} at 2.54Å, which determine the first neighbour distance r_1^{++} = 2.43Å. More significantly the *negative* ω^{++}_{ErB} and ω^{++}_{ErFe} create the deep first minimum in the $RDF^{++}(r)$ at $r \approx 3.3$Å which was described above. The Er-Er first neighbour correlations are also too weak (ω^{++}_{ErEr} = 0.054) to make any significant contribution to $RDF^{++}(r)$ in this

region. These negative contributions from ω_{ErB}^{++} and ω_{ErFe}^{++} reduce the position of the first neighbour peak r_1^{++} ; its half-width and its coordination number n_1^{++} as observed. Intuitively, it seems unphysical that the $RDF^{++}(r)$ could be negative near the deep first minimum. However, Equation 9 shows that the two $RDF^{\pm\pm}(r)$ curves are a weighted sum of the six atomic pair correlation functions $\rho_{AB}^{\pm\pm}(r)$. If one of the $\omega_{AB}^{\pm\pm}$ weighting factors is very large and negative, the $RDF^{\pm\pm}(r)$ can also be negative in the region of the associated r_{AB}.

It is necessary to imagine that the two sets of stick diagrams have been interchanged in Figure 3 (as the ω_{AB}^{++} are in Table 1) to show that the alternative magnetic structure (μ_{Fe} **UP** : μ_{Er} **DOWN**) is inappropriate for the $Fe_{64}Er_{19}B_{17}$ glass at 1.5K. Interchanging the sticks means that the *maximum* of the first peak in the $RDF^{--}(r)$ curve would occur at the same radial distance as the *strong negative* Fe-Er correlations at r_{FeEr} = 3.03Å. The overall peak shape would also be incompatible with the positive Fe-Fe correlations at r_{FeFe} = 2.54Å and the *shallow* first minimum would be inconsistent with the *weak* Er-Er correlations at r_{ErEr} = 3.52Å. Equally, for the $RDF^{++}(r)$ curve, the *strong positive* Er-Er and Er-Er correlations would coincide with the deep first *minimum* and the *weaker* Fe-Fe and Er-B correlations would fail to describe the *maximum* of the first peak at the shorter distance of r_1^{++} = 2.43Å.

Superimposing the stick diagrams of the "correct" magnetic structure on to the $RDF^{--}(r)$, $RDF^{++}(r)$ functions gives an excellent description of the first neighbour peaks which suggests that the structure of the glass must be (to a first approximation) fairly random. These calculations were extended to three more cases which will be presented in the Sections below. Attempts were also made to improve the description of the first peak profile by replacing the "sticks" with Gaussian functions. It proved difficult to select the half-widths of the Gaussians to give a smooth first peak, without having to introduce a convolution to imitate the instrumental resolution. It was also unclear whether the six (*AB*) atomic pair correlation functions should have the same values of half-width or different ones. The Gaussian functions appeared to offer no significant improvement over the stick diagrams and involved substantially more work.

3.2) Compensated sperimagnetism with $\overline{\mu}_{Fe}^{\parallel} = \overline{\mu}_{Er}^{\parallel} = 0$ at T_{comp}.

Initially, the two spin-dependent total structure factors $S^{\pm\pm}(Q)$ were derived from the non spin-flip cross-sections $\frac{\partial\sigma^{\pm\pm}}{\partial\Omega}$ at 112K using the moment values $\overline{\mu}_{Fe}^{\parallel} = 1.13\mu_B$ and $\overline{\mu}_{Er}^{\parallel} = -3.79\mu_B$ which came from the calculations of the spin-flip cross-sections in **Part I**. The two $S^{\pm\pm}(Q)$ were similar in form, except that the heights of the features were greater in the $S^{--}(Q)$. The Fourier Transform of the two structure factors was made using the steps described in Section 2.2. The resulting $RDF^{--}(r)$, $RDF^{++}(r)$ were obviously similar and both had a well-defined first peak at $r_1 \approx 2.7$Å. The $\omega_{AB}^{\pm\pm}$ weighting factors calculated with the $\overline{\mu}_{Fe}^{\parallel} = 1.13\mu_B$ and $\overline{\mu}_{Er}^{\parallel} = -3.79\mu_B$ moment values are given in Table 2. These created the problem of having two different sets of stick-diagrams to describe the virtually identical first peaks in the two $RDF^{\pm\pm}(r)$. The *mean* values $\left\langle \omega_{AB}^{\pm\pm} \right\rangle$ of the weighting factors for the (μ_{Fe} **UP** : μ_{Er} **DOWN**) and (μ_{Fe} **DOWN** : μ_{Er} **UP**) configurations were therefore used to imitate a magnetic structure which might consist of equal volumes of these two configurations at T_{comp}. They are also given in Table 2 and their "sticks" provided a much better representation of the first peak in the two $RDF^{\pm\pm}(r)$.

It was explained in Section 3.2 of **Part I** that the magnetic moment values which were used to calculate the spin-flip cross-sections at 112K, were already different from those obtained from the *general variation* of the magnetisation with temperature. Figure 5 of **Part I** also showed that the temperature variation of the $\left\langle \left(b + p^{\parallel}(Q)\right)\right\rangle^2$, $\left\langle \left(b - p^{\parallel}(Q)\right)\right\rangle^2$ combined scattering amplitudes could be interpreted by the conditions, $\overline{\mu}_{Fe}^{\parallel}$ and $\overline{p}_{Fe}^{\parallel} \to 0$ $\overline{\mu}_{Er}^{\parallel}$ and $\overline{p}_{Er}^{\parallel} \to 0$ at

		$\omega_{AB}^{\pm\pm}$ possible weighting factors for $Fe_{64}Er_{19}B_{17}$ at 112K			
		The magnetic structure is $\overline{\mu}_{Fe}^{\parallel}$ 1.13μ_B UP $\overline{\mu}_{Er}^{\parallel}$ - 3.79 μ_B DOWN		Mean values $\left\langle \omega_{AB}^{\pm\pm} \right\rangle$ for $\overline{\mu}_{Fe}^{\parallel}$ 1.13μ_B $\overline{\mu}_{Er}^{\parallel}$ -3.79μ_B	No moment $\overline{\mu}_{Fe}^{\parallel} = 0.0\mu_B$ $\overline{\mu}_{Er}^{\parallel} = 0.0\mu_B$ $\omega_{AB}^{\pm\pm}$ identical
Pair correlation	r_{AB} in Å	$RDF^{--}(r)$ (*b*+*p*) type	$RDF^{++}(r)$ (*b*-*p*) type		
B-B	1.76	0.011	0.011	0.011	0.011
Fe-B	2.15	0.202	0.104	0.153	0.153
Fe-Fe	2.54	0.896	0.235	0.566	0.515
Er-B	2.64	-0.011	0.087	0.038	0.038
Fe-Er	3.03	-0.101	0.395	0.147	0.252

Er-Er	3.52	0.003	0.164		0.084		0.031

Table 2 Three sets of the ω_{AB} weighting factors which were used to draw the "stick diagrams" on the first peak of the $RDF^{--}(r)$, $RDF^{++}(r)$ functions of $Fe_{64}Er_{19}B_{17}$ at 112K are given. The first two sets are calculated with the moment values $\overline{\mu}_{Fe}^{\parallel}$ = 1.13μ_B, $\overline{\mu}_{Er}^{\parallel}$ = -3.79 μ_B from **Part I**; the third set is their mean value and the fourth set with $\overline{\mu}_{Fe}^{\parallel}$ = $\overline{\mu}_{Er}^{\parallel}$ = 0.0μ_B is calculated from the *b* values alone.

112K which describe a compensated sperimagnetic phase at T_{comp}. A second derivation of the $S^{\pm\pm}(Q)$ structure factors was therefore made using the conditions from Section 3.2 of **Part I**,

$$|\mu_{Fe}| = 1.65\mu_B,\ 2\theta_{\mathrm{Fe}} = 360^{\circ} \text{ with } |\mu_{Er}| = 7.2\mu_B,\ 2\theta_{\mathrm{Er}} = 360^{\circ}.$$

This was different from the example shown in Figure 2a, because there is no Q dependence of the total scattering and Laue-type scattering levels which are horizontal lines at 0.722 barns steradian^{-1} atom^{-1} and 0.024 barns steradian^{-1} atom^{-1} respectively. The $S^{\pm\pm}(Q)$ structure factors from this derivation are shown in Figure 4 and have a pre-peak, an asymmetrical first peak and a second peak without a shoulder. Even though they contain information about the atomic structure alone, they are not expected look like the *S(Q)* of the parental $TM_{83}met_{17}$ glasses at such high erbium concentration. Rather unexpectedly they resemble the structure factor of the high boron glass $^{60}Ni_{64}B_{36}$ [18]

The pre-peak which occurs in both $S^{\pm\pm}(Q)$ structure factors must originate from the atomic structure alone when the conditions $\overline{p}_{Fe}^{\parallel}$ and $\overline{p}_{Er}^{\parallel} = 0$ apply. Using the relation $r_{pp} = \frac{5}{4}\frac{2\pi}{Q_{pp}}$ [19] gives a large radial distance $r_{pp} \approx 6.0$Å, which would be consistent with second

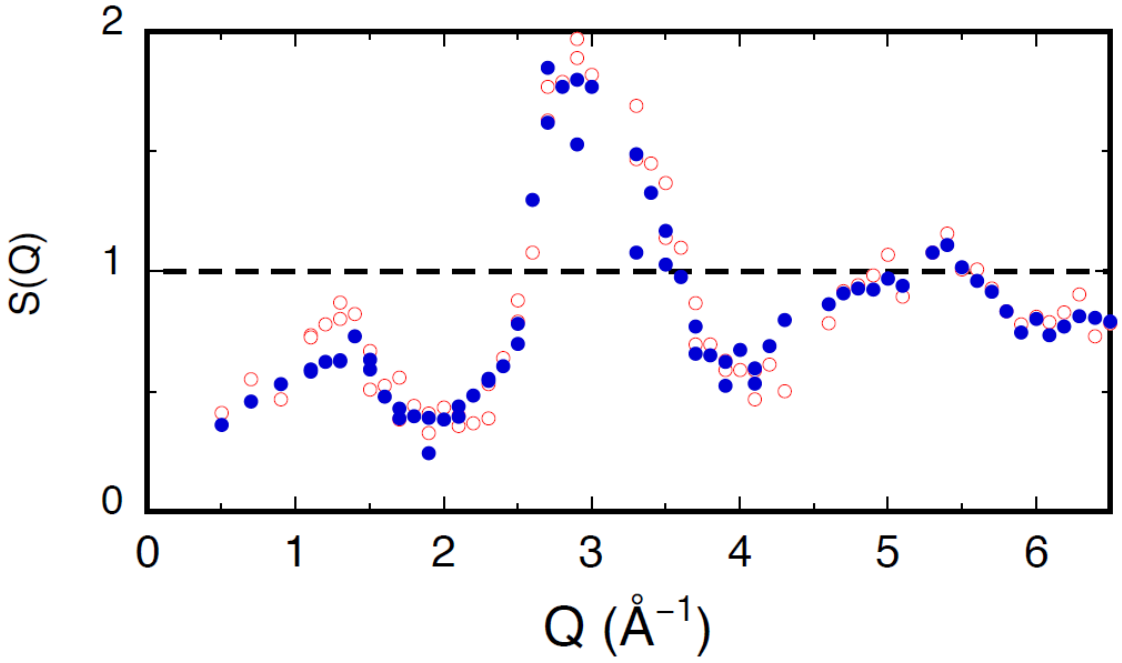

Figure 4 The two spin-dependent total structure factors $S^{\pm\pm}(Q)$ derived from the $\frac{\partial\sigma^{\pm\pm}}{\partial\Omega}$ cross-sections of the $Fe_{64}Er_{19}B_{17}$ glass at 112K, under the conditions $\overline{p}^{\parallel}_{Fe}(Q)$ and $\overline{p}^{\parallel}_{Er}(Q)=0$ are shown.

neighbour erbium atoms≈ 1.7 × 3.54Å in a glassy structure. However, erbium -erbium correlations will not be very visible because the ω_{ErEr} weighting terms are small (see Table 2). "Collineations" of Fe-Er-Fe neighbours which will occur at a distance of 6.06Å are better candidates. These "collineations" were first identified by Bernal in his DRPHS models [20] and also discussed by Cargill [21]. Below T_{comp} the pre-peak is large in $S^{++}(Q)$ and is absent from $S^{--}(Q)$, so it must be associated with atomic AB pair correlations for which ω^{++}_{AB} is large and ω^{--}_{AB} is small. Table 1 shows that Fe-Fe correlations are good candidates which could involve Fe-Er-Fe "collineations".

The average $\langle RDF^{\pm\pm}(r)\rangle$ derived from the two $S^{\pm\pm}(Q)$ is shown Figure 5. The stick-diagrams calculated under the conditions $\overline{p}^{\parallel}_{Fe}$ and $\overline{p}^{\parallel}_{Er}=0$ are superimposed onto the first peak and the $\omega^{\pm\pm}_{AB}$ weighting factors are given in Table 2. They are similar to the $\langle\omega^{\pm\pm}_{AB}\rangle$ values except for ω_{FeEr} and ω_{ErEr}. The six first neighbour sticks calculated with this configuration are all positive and the first peak in the $\langle RDF^{\pm\pm}(r)\rangle$ provides a satisfactory envelope of the sticks.

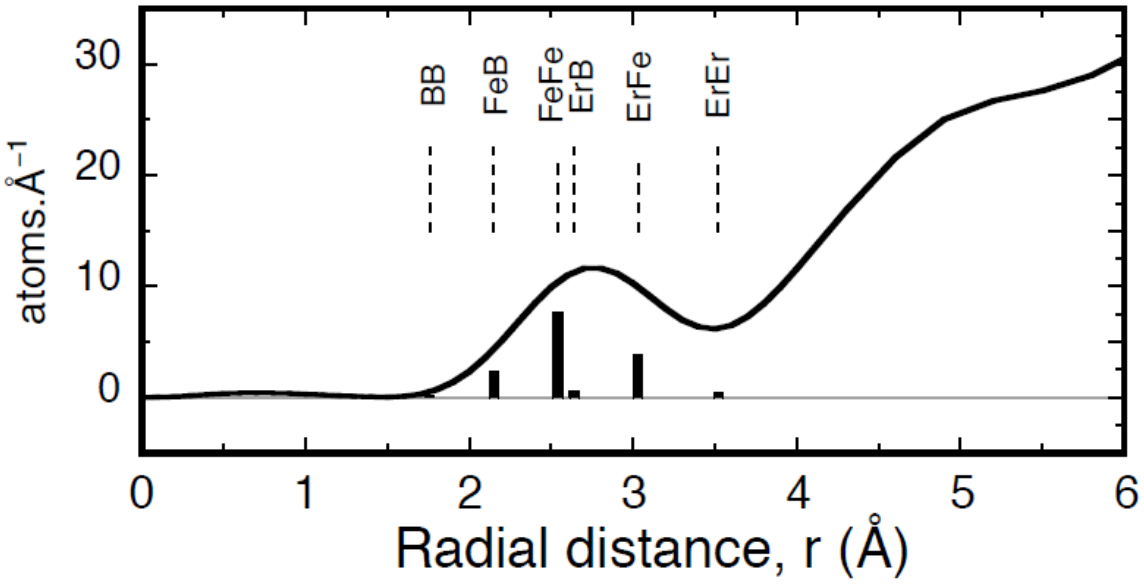

Figure 5 The mean radial distribution function $\langle RDF^{\pm\pm}(r)\rangle$ for the $Fe_{64}Er_{19}B_{17}$ glass at 112K is shown. The stick diagrams for the conditions $\overline{\mu}_{Fe}^{\parallel}$ and $\overline{p}_{Fe}^{\parallel}=0$; $\overline{\mu}_{Er}^{\parallel}$ and $\overline{p}_{Er}^{\parallel}=0$ which describe a compensated sperimagnetic state at T_{comp} are superimposed on the first peak.

The position of this first peak $r_1 = 2.75$Å in the $\langle RDF^{\pm\pm}(r)\rangle$ is determined by the dominant Fe-Fe and Fe-Er correlations at 2.54Å and 3.03Å respectively. It is 5% greater than the weighted mean first neighbour distance in $Fe_{64}Er_{19}B_{17}$ at this temperature and similar to the average ($\langle r_1 \rangle$ = 2.77Å) of the two values r_1^{++} = 2.43Å, r_1^{--} = 3.11Å measured at 1.5K. The coordination number was obtained from the area up to the maximum of the first peak, since the first minimum in the $\langle RDF^{\pm\pm}(r)\rangle$ remains at about the half peak height. The value of n_1 = 12.3 is also consistent with n_1^{--} = 12.0 at 1.5K. Unfortunately, this $\langle RDF^{\pm\pm}(r)\rangle$ does not provide any positive evidence of any "collineations" at $r \approx 6.0$Å. When plotted on an extended scale, the positions of its maxima are at 2.75Å, 4.9Å, 7.0Å and 9.4Å, so that $r \approx$ 6.0Å lies between the second and third of these. This minimum is actually quite *shallow* and this may be consistent with the fact that the pre-peak is sufficiently weak ($S(Q_{pp}) \leq 1.0$) at 112K that it cannot produce a *positive* feature in the $\langle RDF^{\pm\pm}(r)\rangle$ at $r \approx 6.0$Å.

3.2) Sperimagnetism in $Fe_{64}Er_{19}B_{17}$ above T_{comp} and in $Fe_{78}Er_5B_{17}$ at 2K.

The two spin-dependent total structure factors $S^{++}(Q)$, $S^{--}(Q)$ and their associated $RDF^{++}(r)$, $RDF^{--}(r)$ were also obtained from the $\frac{\partial\sigma^{++}}{\partial\Omega}$, $\frac{\partial\sigma^{--}}{\partial\Omega}$ cross-sections of the $Fe_{64}Er_{19}B_{17}$ glass at 180K and of $Fe_{78}Er_5B_{17}$ at 2K. The contributions from the magnetic neutron scattering are smaller in these cross-sections, because of the higher temperature and the reduced concentration of erbium respectively. It was of interest to see whether the expected magnetic structure (μ_{Fe} **UP** : μ_{Er} **DOWN**), could be identified effectively in these two cases. Figure 6 shows the $RDF^{--}(r)$ and $RDF^{++}(r)$ for the $Fe_{64}Er_{19}B_{17}$ glass at 180K, together with the stick diagrams calculated for the (μ_{Fe} **UP** : μ_{Er} **DOWN**) magnetic structure whose $\omega_{AB}^{\pm\pm}$ weighting factors are given in Table 3.

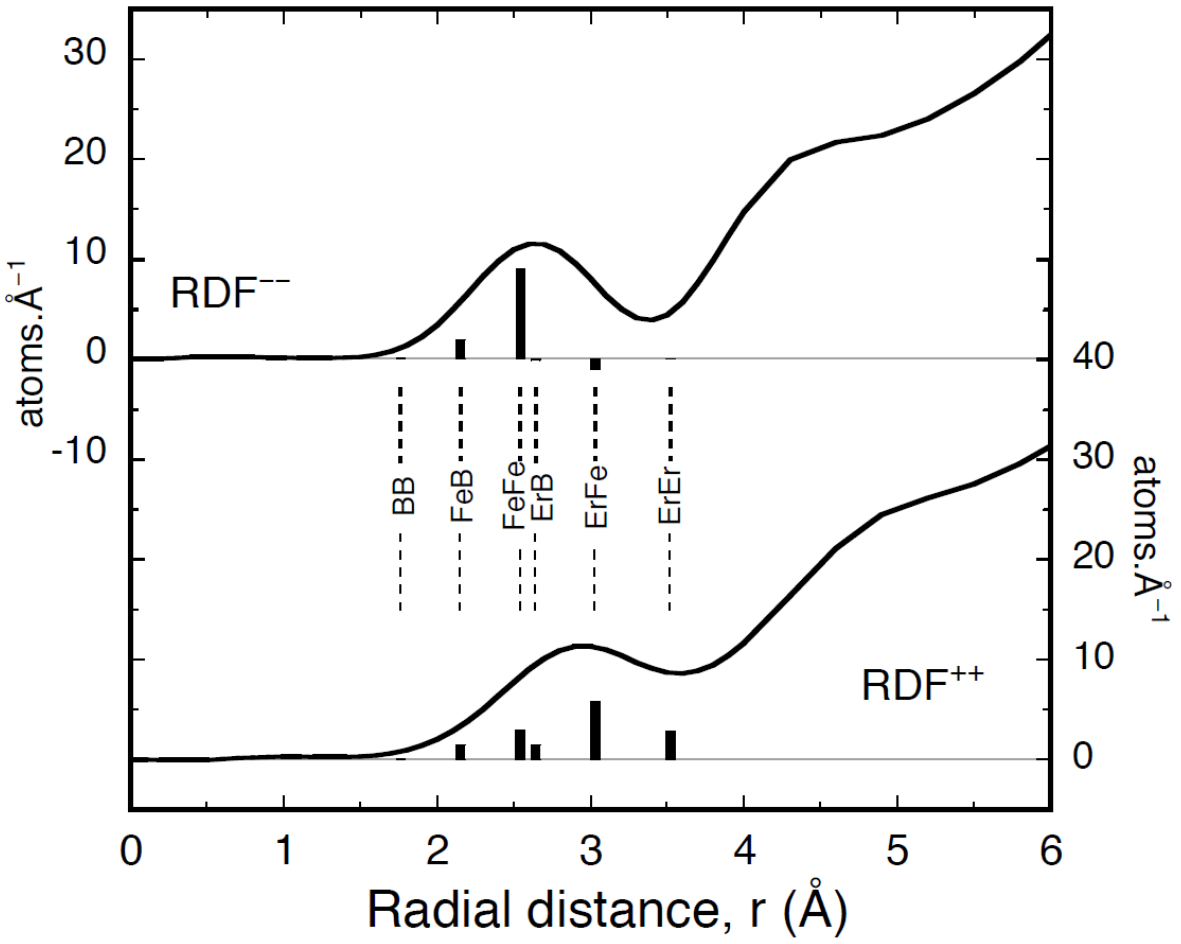

Figure 6 The $RDF^{--}(r)$ and $RDF^{++}(r)$ functions of the $Fe_{64}Er_{19}B_{17}$ glass at 180K are shown. The stick diagrams were calculated with the (μ_{Fe} **UP** : μ_{Er} **DOWN**) structure and the $\omega_{AB}^{\pm\pm}$ weighting factors from Table 3.

Comparing Figures 3 and 6, shows that the derived $RDF^{\pm\pm}(r)$ and the stick diagrams have interchanged, because the magnetic structure has inverted. The first peak of $RDF^{++}(r)$ in Figure 6 again provides a good envelope of the six first neighbour sticks, which are all positive. It has moved to a slightly *smaller* distance r_1^{++} = 2.92Å compared with r_1^{--} = 3.11Å in $RDF^{--}(r)$ at 1.5K because of substantial changes in the ω_{FeFe} and ω_{ErEr} weighting factors between 1.5K and 180K. The first minimum in $RDF^{++}(r)$ at 180K has the same depth as in $RDF^{--}(r)$ at 1.5K. The first peak in the $RDF^{--}(r)$ is at r_1^{--} = 2.62Å and the first minimum less deep because the *negative* ω_{ErB} and ω_{FeEr} weighting factors are only ≈ 19% of their values at 1.5K. The positions of the first peak in the two *RDF*s, r_1^{++} = 2.92Å ; r_1^{--} = 2.62Å are much closer than they were at 1.5K, but their average $\langle r_1 \rangle$ = 2.77Å is the same and close to the (single) value r_1 = 2.75Å at 112K. The two coordination numbers, n_1^{++} = 11.9 ; n_1^{--} = 11.4 are also closer because the reduction in ω_{ErB} and ω_{FeEr} produces less distortion in the shape of the first peak. The mean coordination number for the $Fe_{64}Er_{19}B_{17}$ glass obtained from those *RDF*s at 1.5K, 112K and 180K which have a positive set of the six ω_{AB} was $n_1 = 12.1 \pm 0.2$.

		$\omega_{AB}^{\pm\pm}$ weighting factors for $Fe_{64}Er_{19}B_{17}$ at 180K			$\omega_{AB}^{\pm\pm}$ weighting factors for $Fe_{78}Er_5B_{17}$ at 2K	
		Magnetic structure μ_{Fe} **UP** μ_{Er} **DOWN**			Magnetic structure μ_{Fe} **UP** & μ_{Er} **DOWN**	
Pair correlation	r_{AB} in Å	or $RDF^{++}(r)$ (*b-p*) type	for $RDF^{--}(r)$ (*b+p*) type		for $RDF^{++}(r)$ (*b-p*) type	for $RDF^{--}(r)$ (*b+p*) type
B-B	1.76	0.013	0.010		0.024	0.006
Fe-B	2.15	0.102	0.192		0.184	0.154
Fe-Fe	2.54	0.202	0.905		0.358	0.961
Er-B	2.64	0.099	-0.010		0.079	-0.009
Fe-Er	3.03	0.393	-0.099		0.296	-0.116
Er-Er	3.52	0.191	0.003		0.061	0.003

Table 3 The interatomic pair distances r_{AB} are given in ascending order with the ω_{AB} weighting factors calculated for the $Fe_{64}Er_{19}B_{17}$ at 180K and $Fe_{78}Er_5B_{17}$ at 2K

It was explained in Section 2.0, that the non spin-flip cross-sections of the $Fe_{78}Er_5B_{17}$ glass at 2K were somewhat similar to the spin-dependent cross-sections of $Co_{81}P_{19}$ [13]; $Co_{81.5}B_{18.5}$

[14]; $Fe_{83}B_{17}$ [15] and $(Fe,Tb)_{83}B_{0.17}$ [3] type glasses. They are quite different from those of the $Fe_{64}Er_{19}B_{17}$ glass at 1.5K described in Section 2.1, whose two total scattering levels had similar values in the forward limit Q = 0 and both decreased with increasing Q. The total scattering level $\left\langle \left(b+p^{\parallel}(Q)\right)^2 \right\rangle$ for $Fe_{78}Er_5B_{17}$ at 2K has a forward limit $\left\langle \left(b+p^{\parallel}(0)\right)^2 \right\rangle$ = 1.78 barns steradian^{-1} atom^{-1} and *falls* rapidly with Q, while $\left\langle \left(b-p^{\parallel}(Q)\right)^2 \right\rangle$ has a much smaller forward limit $\left\langle \left(b-p^{\parallel}(0)\right)^2 \right\rangle$ = 0.631 barns steradian^{-1} atom^{-1} and actually *increases* with Q as observed for the other glasses [12,13,14]. Because of these differences, the features in the $S^{++}(Q)$, $S^{--}(Q)$ structure factors of the $Fe_{78}Er_5B_{17}$ glass turn out to be much less well developed than those of the $Fe_{64}Er_{19}B_{17}$ sample.

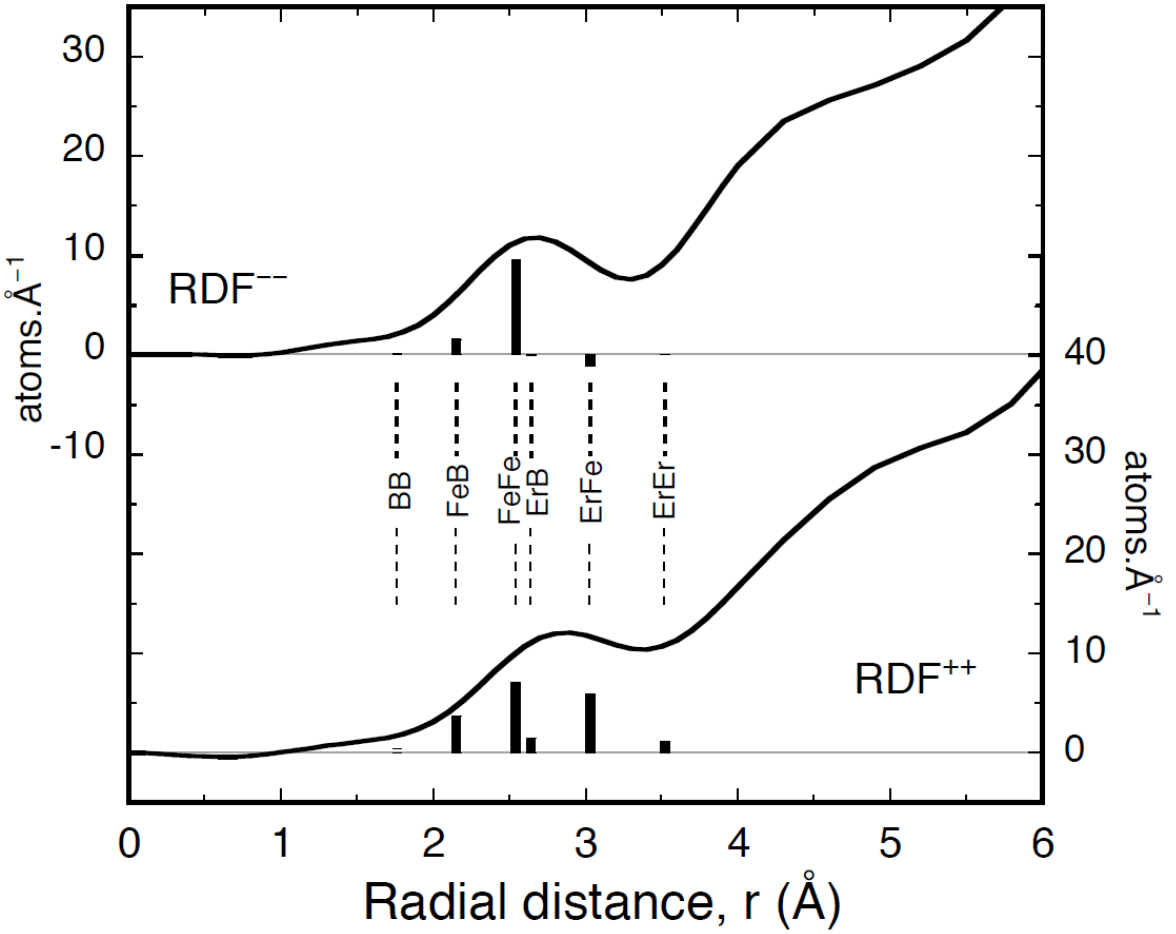

Figure 7 The $RDF^{--}(r)$ and $RDF^{++}(r)$ functions of the $Fe_{78}Er_5B_{17}$ glass at 2K are shown. The stick diagrams were again calculated with the (μ_{Fe} **UP** : μ_{Er} **DOWN**) structure with the $\omega_{AB}^{\pm\pm}$ weighting factors from Table 3. Despite the lower concentration of erbium, they continue to provide a good description of the profiles of the first neighbour peaks.

Figure 7 shows the derived $RDF^{--}(r)$ and $RDF^{++}(r)$ for $Fe_{78}Er_5B_{17}$ at 1.5K and the stick diagrams show again that the (μ_{Fe} **UP** : μ_{Er} **DOWN**) configuration is the correct magnetic structure. Table 3 gives the corresponding $\omega_{AB}^{\pm\pm}$ weighting factors which are by coincidence, rather similar to those of the $Fe_{64}Er_{19}B_{17}$ glass at 180K. Even with this similarity, quite subtle differences between the derived parameters such as r_1^{++} = 2.86Å, r_1^{--} = 2.62Å in $Fe_{78}Er_5B_{17}$ at 2K compared with r_1^{++} = 2.92Å, r_1^{--} = 2.63Å in $Fe_{64}Er_{19}B_{17}$ at 180K, can be explained by the small differences in their $\omega_{AB}^{\pm\pm}$ weighting factors . The coordination number n_1 = 12.6 for $Fe_{78}Er_5B_{17}$ obtained from the $RDF^{++}(r)$ which has all the ω_{AB}^{++} positive, is slightly larger than that of $Fe_{64}Er_{19}B_{17}$, but the atomic packing in these ternary glasses is probably easier when the concentration of the erbium is small. The chief difference between the *RDF*s of these two glasses is that the features in those of $Fe_{78}Er_5B_{17}$ are less well developed than in $Fe_{64}Er_{19}B_{17,}$ - as illustrated by the depth of the first minimum in both $RDF^{++}(r)$, $RDF^{--}(r)$. This is partly because the features in $S^{\pm\pm}(Q)$ of the $Fe_{78}Er_5B_{17}$ glass are less well developed, as already explained, but also because the atomic number density of $Fe_{78}Er_5B_{17}$ is ≈ 23% greater than that of $Fe_{64}Er_{19}B_{17}$. The parabolic background $4\pi\rho_0 r^2$ of its *RD*Fs is ≈ 2.5 atoms Å^{-1} greater by $r \approx 3.5$Å, which is similar to the difference in depth of the first minimum in the *RDF*s.

4) Conclusions

The two sets of polarised beam neutron scattering measurements we have made on the on $Fe_{78}Er_5B_{17}$ and $Fe_{64}Er_{19}B_{17}$ glasses proved for a while, to be difficult to interpret. Part of this was due to the complexity of their non-collinear ferrimagnetic structures. The inability to *simulate* the non spin-flip neutron scattering cross-sections (especially those of the $Fe_{64}Er_{19}B_{17}$ glass), led to their analysis using a Fourier transform. Two spin-dependent total structure factors $S^{\pm\pm}(Q)$ were first defined from the non spin-flip scattering cross-sections $\frac{\partial\sigma^{\pm\pm}}{\partial\Omega}$. Their Fourier transform gave two spin-dependent Radial Distribution Functions $RDF^{\pm\pm}(r)$ which could be interpreted in terms of the (six) atomic pair correlation functions $\rho_{AB}^{\pm\pm}(r)$ and their respective weighting factors $\omega_{AB}^{\pm\pm}$. This has produced a coherent description

of the atomic-scale magnetic structures in the $(Fe,Er)_{83}B_{17}$ glasses, despite the limited range of the scattering data in the Fourier transform.

The very large magnetic scattering amplitude of erbium, (*e.g.* $\left|p^{\parallel}_{Er}(0)\right| = 17.73$ fm at 1.5%K) has been the most significant parameter in determining the form of the neutron scattering cross-sections. It has generated a wide range in the values of the combined scattering amplitudes $\left(b \mp p^{\parallel}(Q)\right)$ and both positive and negative values of the $\omega^{\pm\pm}_{AB}$ weighting factors, which were the key to interpreting the position and shape of the first peak in the $RDF^{\pm\pm}(r)$.

An important feature of the Fourier transforms is that they have not involved any adjustable parameters, since the nuclear scattering amplitudes are tabulated and the $\overline{\mu}^{\parallel}_{Fe}$, $\overline{\mu}^{\parallel}_{Er}$ components of the magnetic moments (which define the magnetic scattering amplitudes) came directly from the magnetisation data in **Part I**. In addition, the scattering cross-sections had been derived *in absolute units* from the raw data using our own programs.

The main conclusions from **Parts I** and **II** of this work are as follows. First, the (bulk) magnetisation measurements have confirmed that the ferromagnetic compensation in $Fe_{64}Er_{19}B_{17}$ glass is characterised by an equality of the magnetic sublattices. Second, the interchange of the non spin-flip neutron scattering cross-sections $\frac{\partial\sigma^{++}}{\partial\Omega}, \frac{\partial\sigma^{--}}{\partial\Omega}$ between 100K and 125K which preserves their overall shape, confirms that there is a complete reversal of the atomic-scale magnetic structure at T_{comp}. Third, the convergence of the two non spin-flip cross-sections $\frac{\partial\sigma^{++}}{\partial\Omega}, \frac{\partial\sigma^{--}}{\partial\Omega}$ at 112K illustrates that the collinear components of the magnetic moments $\left\langle\mu^{\parallel}_{Er}\right\rangle$, $\left\langle\mu^{\parallel}_{Fe}\right\rangle$ go to zero in a special, compensated sperimagnetic phase which appears to exist at exactly T_{comp}. Finally, the presence of the pre-peak at $Q_{pp} \approx 1.3$Å^{-1} in the spin-dependent total structure factors $S^{\pm\pm}(Q)$ at 112K, shows that it must originate in the atomic structure and may probably involve Fe-Er-Fe "collineations" at a radial distance of about 6.0Å.

5) Acknowledgements

The neutron experiments were made within the EPSRC Neutron Beam programme and the help of the staff at the Institut Laue-Langevin, particularly Drs J Kulda and M Enderle, is gratefully acknowledged. The authors would also like to thank Dr N Al-Senany who checked

the derivation of the spin-dependent Structure Factors and their Fourier transform with her own, independent computer codes.

References

[1] Wildes A R and Cowlam N Recent Research Developments in Magnetism and Magnetic Materials 2003 **1** 541-563.

[2] Wildes A R and Cowlam N 2011 Part I

[3] Cowlam N, Hanwell M D, Wildes A R and Jenner A G I 2005 J Phys : Condens Matter **17** 3585-3596.

[4] Krishnan R, Lassri H and Teillet J 1991 JMMM **98** 155-61.

[5] Benjelloun J, Baran M, Lassri H, Oukris H, Krishnan R, Omri M and Ayadi M 1999 JMMM **204** 68-72.

[6] García L M, Pizzini S, Rueff J P, Vogel J, Galér, Fontaine A, Kappler J P, Krill G and Goedkoop J B 1996 J Appl Phys **79** 6497-99.

[7] Pizzini S, García L M, Fontaine A, Rueff J P, Vogel J, Galéra R M Goedkoop J B, Brookes N B, Krill G and Kappler J P 1997 J of Elec Spect **86** 165-73

[8] Szymański K, Kalska B, Satuła D, Dobrzyński L, Brodderfalk A, Wäppling R, and Nordblad P 2002 JMMM **251** 271-82.

[9] Cowlam N, Wildes A R, Hanwell M D, Dearing N and Jenner A G I J Phys : Condens Matter 2010 **22** 296003

[10] Halpern O and Johnson M N 1939 Phys Rev **55** 898-923

[11] http://www.ncnr.nist.gov/resources/n-lengths

[12] Blétry J and Sadoc J F 1975 J Phys F : Metal Phys **5** L111-7.

[13] Dubois J M, Chieux P, Le Caer G, Schweitzer J and Blétry J 1982 J de Physique **C9** 23-9

[14] Guoan Wu, Cowlam N, Davies H A, Cowley R A, Paul D McK and Stirling W G, 1982 J de Physique **12** C71-76

[15] Brown P J 1995 International Tables for Crystallography
ed Wilson A J C (Dordrech : Kluwer) Vol **C** 391.

[16] Faber T E and Ziman J JM 1965 Phil Mag **11** 153-73

[17] Lorch E 1969 J Phys C : Solid St **2** 229-37

[18] Gardner P P, Cowlam N and Davies H A 1985 **15** J Phys F : Met Phys **15** 767-78

[19] Klug H P and Alexander L E 1974 X-ray diffraction procedures (John Wiley : New York)

[20] Bernal J D 1964 Proc. Roy Soc **A280** 299

[21] Cargill G S III 1975 Solid State Physics 30 227-320